

Composite Layers for Deep Anomaly Detection on 3D Point Clouds

Alberto Floris, Luca Frittoli, Diego Carrera, and Giacomo Boracchi

Abstract—Deep neural networks require specific layers to process point clouds, as the scattered and irregular location of points prevents us from using convolutional filters. Here we introduce the composite layer, a new convolutional operator for point clouds. The peculiarity of our composite layer is that it extracts and compresses the spatial information from the position of points before combining it with their feature vectors. Compared to well-known point-convolutional layers such as those of ConvPoint and KPConv, our composite layer provides additional regularization and guarantees greater flexibility in terms of design and number of parameters. To demonstrate the design flexibility, we also define an aggregate composite layer that combines spatial information and features in a nonlinear manner, and we use these layers to implement a convolutional and an aggregate CompositeNet. We train our CompositeNets to perform classification and, most remarkably, unsupervised anomaly detection. Our experiments on synthetic and real-world datasets show that, in both tasks, our CompositeNets outperform ConvPoint and achieve similar results as KPConv despite having a much simpler architecture. Moreover, our CompositeNets substantially outperform existing solutions for anomaly detection on point clouds.

I. INTRODUCTION

PPOINT CLOUDS provide a compact yet detailed representation of 3D objects and, for this reason, they are widely employed in several applications such as autonomous driving [1], [2], topography [3], architecture and heritage preservation [4]. Point clouds are unordered sets of points in \mathbb{R}^3 , typically acquired by LiDAR sensors [3], [1] or depth cameras [5], which are sometimes paired with features like the color or the normal vector to the surface of the object [6].

The design of deep neural networks that can process *point clouds* has been attracting more and more interest in 3D deep learning [7], starting from *PointNet* [6]. Such a flourishing literature is motivated by the intrinsic challenges of training machine learning models on point clouds. In fact, unlike images, point clouds cannot be arranged on a regular grid, where it is possible to define convolutional filters. For this reason, several *point-convolutional* layers, namely layers implementing convolutions on point clouds, have been proposed, two relevant examples being *ConvPoint* [8] and *KPConv* [9].

Deep learning research on point clouds has primarily addressed *supervised* tasks such as classification or part segmentation [8], [9], [10], [11], [12], [13], while *unsupervised*

A. Floris is with Skyqraft AB, Stockholm, Sweden. Part of this work was done during a postgraduate internship at STMicroelectronics.

L. Frittoli and G. Boracchi are with Politecnico di Milano, Dipartimento di Elettronica, Informazione e Bioingegneria, Milan, Italy.

D. Carrera is with STMicroelectronics, Systems Research and Applications, Agrate Brianza, Italy

Manuscript received .

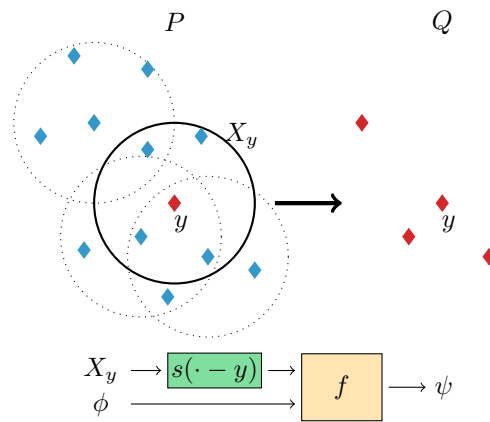


Fig. 1. Our composite layer: the spatial function s outputs a vector in \mathbb{R}^K for each point x belonging to the convolution window X_y , where y is the output point. The semantic function combines the input features ϕ and the output of the spatial function $\{s(x - y)\}_{x \in X_y}$ to produce the output feature vector $\psi(y)$.

problems have been much less investigated. Moreover, most of the *anomaly detection* algorithms for point clouds concern very specific scenarios [14], [15], and typically resort to *ad-hoc* feature extractors. Needless to say, many industrial and quality inspection scenarios would benefit from effective deep neural networks for anomaly detection on point clouds since these do not require feature engineering. To the best of our knowledge, the only deep learning solution for anomaly detection on point clouds is a variational autoencoder [16].

In this work we propose a novel *composite layer* (Fig. 1), which is a flexible alternative to the existing point convolutions in deep neural networks for point clouds. We define the composite layer as the composition of two learnable functions defined over each *convolution window* X_y , namely a neighborhood of each point y of the output point cloud. The first, called *spatial function* s , extracts and compresses the information from the spatial arrangement of the points in X_y . The second, called *semantic function* f , combines the spatial information extracted by s with the feature vectors $\phi(x) \in \mathbb{R}^I$ associated to each point $x \in X_y$. Similarly to convolutional layers in CNNs for images, our semantic function stacks J filters that share the spatial information and produce the output features $\psi(y) \in \mathbb{R}^J$. By compressing the spatial information through s before combining it with the features, our composite layer adds a form of regularization compared to the point-convolutional layers from the literature.

Another major advantage of the composite layer is that

the spatial and semantic functions can be customized independently, guaranteeing a remarkable flexibility in terms of design and number of parameters. We present two types of composite layer that combine spatial information and features in substantially different ways, to demonstrate its design flexibility. Besides the *convolutional composite layer*, which represents an alternative formulation for point convolution, we present the *aggregate composite layer*, which combines spatial information and features in a nonlinear manner, while most of the existing works exclusively adopt linear operators.

Existing point-convolutional layers such as the well-established ConvPoint [8] and KPConv [9] lack a similar flexibility since their components operating on spatial information and features are tightly related by design. For this reason, they cannot be easily customized without compromising the performance of the network or substantially increasing the number of parameters, as we demonstrate in our experiments.

We use our composite layers to implement *CompositeNets*, which can be successfully employed in both supervised tasks such as classification and, most importantly, unsupervised anomaly detection on point clouds. To this purpose, we train our CompositeNets for anomaly detection following the self-supervised approach presented in [17], using geometric transformations to produce surrogate labels. Our code is publicly available at <https://github.com/sirolf-otrebala/CompositeNet>.

Our experiments on two synthetic point cloud benchmarks, namely *ModelNet40* [18] and *ShapeNet* [19], and the real-world *ScanNet* dataset [5] show that our aggregate CompositeNet outperforms ConvPoint and achieves similar classification performance compared to KPConv [9] despite having a much simpler architecture. We also show that self-supervised deep neural networks substantially outperform both traditional anomaly detectors based on hand-crafted point cloud descriptors [20] and the variational autoencoder presented in [16], which is the only deep anomaly-detection algorithm for point clouds in the literature. As for classification, our experiments on anomaly detection indicate that our aggregate CompositeNet outperforms ConvPoint and aligns with KPConv despite having a much simpler architecture. These promising results confirm the effectiveness of our composite layers.

To summarize, our key contributions are:

- We define the composite layer, a new layer for point-cloud processing in neural networks that is more flexible than the existing point-convolutional operators.
- We implement convolutional and aggregate (nonlinear) composite layers to be used as building blocks for CompositeNets.
- Our self-supervised CompositeNets achieve state-of-the-art anomaly detection performance on synthetic and real-world point cloud benchmarks.

The rest of the paper is organized as follows: in Section II we review the literature on deep learning for point clouds, with a focus on point convolutions and anomaly detection. In Section III we formulate the desired point-convolutional layer and state the anomaly-detection problem, while in Section IV we illustrate in detail how point convolution has been implemented in most of the literature. Then, in Section V we present our convolutional and aggregate composite layers, and

empirically demonstrate their superior design flexibility with respect to existing point-convolutional layers. In Section VI we present and discuss our experimental results in the classification and anomaly-detection tasks, and finally in Section VII we give some conclusive remarks and illustrate future research directions.

II. RELATED WORK

The first deep-learning methods for point clouds cope with their scattered nature by projecting the 3D points on several planes [22], thus generating 2D images that can be processed by traditional CNNs. In *volumetric CNNs* [23], 3D point clouds are mapped to a voxel grid, and then processed by 3D convolutional filters. Both approaches imply a loss of information. Moreover, the computational cost of volumetric convolutions scales very poorly with the grid resolution. *Submanifold sparse convolutional networks* [24] represent an efficient alternative that can handle higher-resolution voxel grids by leveraging the sparse nature of point clouds.

In what follows we overview deep-learning techniques operating directly on 3D point clouds without projections or voxelization, with a focus on point-convolutional layers. We refer to [7] for a more comprehensive review on deep learning for 3D point clouds. Moreover, we briefly survey unsupervised anomaly-detection techniques, in particular those designed for 3D point clouds, since this is a fundamental task we address in this work.

A. Deep Learning on Point Clouds

Early approaches. *PointNet* [6] is the first deep neural network directly processing 3D point clouds using Multi-Layer Perceptrons (MLPs) and permutation-invariant pooling. The major drawback is that PointNet feeds the entire point cloud to the same MLP and thus might fail at recognizing local structures inside the point cloud. A straightforward improvement implemented in *PointNet++* [10] is to hierarchically apply PointNet to nested partitions of the point cloud.

Point Convolutions. Due to the success of CNNs in several deep learning tasks involving images, recent works define *point-convolutional layers* operating similarly to convolutional filters on images. In this direction, *volumetric convolutions* [11] are defined by interpolating a 3D function with the input point cloud. Other methods approximate continuous convolutional filters by MLPs [25], [26] or polynomials [12].

A wide variety of point-convolutional layers have been proposed in the literature. However, the vast majority of these layers resort to two mainstream approaches to handle point clouds, which consist in feeding the coordinates of the points to either a *Radial Basis Function Network* (RBFN) or a *Multi-Layer Perceptron* (MLP). We illustrate two prominent examples for these approaches, namely *KPConv* [9] and *ConvPoint* [8], and the other relevant solutions following their path.

The most representative solution following the first approach is KPConv [9], which uses an RBFN to process the coordinates of the points in a window X_y (relatively to the position of the output point y) and then linearly combines

the output tensor of the RBFN with the input features. KPConv and its extension *AGMMConv* [27] also implement a deformable convolutional kernel that adaptively defines the RBFN centers depending on the output point where the kernel is applied. *InterpCNN* [28] is very similar to KPConv, the only difference being the chosen RBFs. *FPCConv* [29] assumes that point clouds represent locally flat surfaces, thus locally projects 3D points to the tangent plane to an estimated surface. Then, FPCConv processes the projected points by a 2D RBFN whose centers are positioned on a regular grid, similarly to KPConv.

The most representative layer defined by MLPs is *ConvPoint* [8]. This operator feeds an MLP with the relative coordinates of the points with respect to a set of centers, which play a similar role as the RBFN centers in KPConv and other layers. Then, the MLP outputs are linearly combined with the input features. *RS-CNN* [30] and *RPNet* [31] follow a similar approach but are not convolutional since the input of their MLPs includes the absolute position of the points, while all point-convolutional layers consider the relative position of the points with respect to the output. *DensePoint* [32] is similar to RS-CNN, the main difference being that the processing of the features does not depend on the relative position of the points with respect to the output point.

The structure and the number of parameters of KPConv, ConvPoint, and the other layers described above depend primarily on the number of centers. In contrast, our composite layer enables more flexibility since we can independently customize the processing of the coordinates of the points (spatial information) and that of the associated features. Moreover, composite layers can aggregate spatial information and features by more general operations than linear combinations. To the best of our knowledge, the only layer that fully separates spatial and feature operations, enabling more flexibility than the solutions described above, is *PACConv* [33]. However, we do not consider this in our experiments because this layer is defined by a sophisticated neural network taking as input the absolute position of the points, thus it is not a point-convolutional operator.

Graph Neural Networks. Another approach consists in processing point clouds by *Graph Neural Networks* (GNNs) [34], [35], [36], [37], [38], [39], which can be considered an extension of PointNet. A relevant example is *Dynamic Graph CNN* (DGCNN) [35], where a graph is defined by connecting some points sampled from the input point cloud to their nearest neighbors, and then processed by a GNN. The major difference between GNNs and point-convolutional networks is that, in GNNs, the coordinates of the points are considered as features associated with the graph vertices and thus are modified by the network layers. In contrast, point-convolutional layers preserve the coordinates of the points and modify only the associated features.

B. Unsupervised Anomaly Detection on Point Clouds

Unsupervised anomaly detection is a challenging problem that has been often addressed by deep learning models. The most popular anomaly detection solutions in the literature

leverage autoencoders [40], GANs [41] or Deep SVDD [42] and its extension DROCC [43], which represent the deep learning counterpart of the well-known SVDD [44]. Another approach leverages pre-defined geometric transformations to perform anomaly detection in a self-supervised fashion [17], or directly learn domain-specific transformations from the training data [45]. We refer to [46] for a more comprehensive survey on anomaly detection.

All these solutions have been designed for anomaly detection in signals or images, and have rarely been used to address anomaly detection on point clouds. In fact, the deep-learning research on point clouds mostly considers supervised settings, and much fewer works address unsupervised learning on point clouds. Among these, the vast majority only tackle very specific industrial monitoring problems such as detecting defective products in additive manufacturing [14]. Other works apply unsupervised clustering to recognize vehicles in autonomous driving [1], or One-Class SVM to identify geometric structures [3], [15] such as poles [15] from point clouds acquired by LiDAR. In general, all unsupervised machine-learning solutions for point clouds rely on hand-crafted features also referred to as *point cloud descriptors* [20]. However, as it turns out in our experiments, these descriptors do not generalize well for anomaly detection. In contrast, our deep neural networks perform anomaly detection following the self-supervised approach in [17], which enables to extract data-driven features that can effectively describe a wider variety of point clouds, resulting in a more general approach. To the best of our knowledge, the only deep learning method for anomaly detection on point clouds is a variational autoencoder [16], and the other existing autoencoders for point clouds [47], [48], [49] do not address anomaly detection.

III. PROBLEM FORMULATION

We define a *point cloud* as a pair (P, ϕ) , where $P \subset \mathbb{R}^d$ is a set of points in a d -dimensional space (in our case $d = 3$), and $\phi : P \rightarrow \mathbb{R}^J$ is a function associating a feature vector $\phi(x) \in \mathbb{R}^J$ (e.g., an RGB triplet) to each point $x \in P$. Our goal is to design a new point-convolutional layer that takes as input (P, ϕ) and returns another point cloud (Q, ψ) , where $Q \subset \mathbb{R}^d$ and $\psi : Q \rightarrow \mathbb{R}^J$. The new layer has to enable a flexible design, where we can independently set the structure and number of parameter of the components handling the spatial information and the features.

The new layer will be used as building block for deep neural networks for classification and, most remarkably, for unsupervised anomaly detection. In the latter case, the training set contains only instances from a single class, considered as *normal*, and the goal is detecting anomalous point clouds, i.e. those that do not belong to the normal class, during testing¹.

IV. BACKGROUND ON POINT CONVOLUTION

Before introducing the proposed composite layer and CompositeNets, we present some background on point convolution.

¹This setup is sometimes referred to as *semi-supervised* since only normal instances are provided for training.

A. Convolution Window and Output Point Cloud

Point-convolutional operators take as input a point cloud (P, ϕ) and return another point cloud (Q, ψ) . As for 2D convolutional filters, the feature vector $\psi(y)$ associated to each output point $y \in Q$ is obtained by processing a *convolution window* $X_y \subset P$. While the grid structure of 2D images makes these operations straightforward, when working on point clouds there are multiple ways to define both the output point $y \in Q$ and the corresponding window $X_y \subseteq P$.

Typically, point-convolutional layers first select each output point $y \in Q$ and then define the convolution window X_y . A popular approach to select y is random sampling from P , which implies that $Q \subseteq P$ [11], [8]. In [8], the points are sampled with replacement from P , but, during sampling, points $y \in P \cap Q$ or points $y \in P$ that are close to points in Q are assigned a lower probability. When applying convolution, the cardinality of the point cloud can be reduced by sampling fewer output points than there are in the input point cloud, i.e. $|Q| < |P|$, which is similar to having a stride in standard convolutions. The convolution window X_y can be defined either as a sphere $X_y := \{x \in P : \|x - y\| < \rho\}$ [9], or as a set containing a fixed number of nearest neighbors of y in P [8]. The two methods can be considered equivalent when the input point cloud P has uniform density [50].

B. Point-Convolutional Operator

After defining the output point y and the corresponding convolution window X_y , the point-convolutional operator [9], [12], [26] is typically defined at each $y \in Q$ as:

$$\psi_j(y) = (\phi * g_j)(y) = \sum_{x \in X_y} \sum_{i=1}^I \phi_i(x) g_{ij}(x - y), \quad (1)$$

where $\phi_i(x)$ is the i -th input feature associated to x and $\psi_j(y)$ is the j -th output feature associated to y . Similarly to CNNs for images, each point-convolutional layer stacks J *filter functions* $g_j : \mathbb{R}^d \rightarrow \mathbb{R}^I$, each having I components (like the input feature function ϕ), denoted by g_{ij} .

Filters in CNNs are learnable weight matrices and their spatial extension corresponds to size of the convolution window. Therefore, each weight is associated to a spatial location and is multiplied to the features of the pixel in the corresponding location of the convolution window. When operating on images, the spatial locations of weights and pixels is inherited from the grid structure of the image. In contrast, point clouds lack such grid structure, and the filter g_j is necessarily a function defined over \mathbb{R}^d .

As stated in Section II, the vast majority of the point-convolutional layers in the literature operate very similarly to either ConvPoint [8] or KPConv [9], which we illustrate here more in detail. Both these layers implement each component of the filter function g_{ij} as a linear combination:

$$g_{ij}(x - y) = \sum_{m=1}^M \tilde{w}_{ijm} H_m(x - y), \quad (2)$$

where \tilde{w}_{ijm} are learnable weights associated to a set of spatial locations $\{c_m\}_{m=1}^M \subset \mathbb{R}^d$, called *centers*, and H_m are

correlation functions, each depending on the relative position of $x - y$ with respect to c_m [9]. This formulation is inspired by convolution on images, where $x - y$ represent the pixel locations in the convolution window X_y , $\{c_m\}$ represent the spatial positions of the weights, and H_m is the Kronecker function $H_m = \delta(x - y, c_m)$, i.e. $\delta(x - y, c_m) = 1$ if $x - y = c_m$ and 0 otherwise [8]. Due to the scattered position of the points in X_y , in point-convolutional layers H_m must be a continuous function, and the position of each center c_m is either a fixed [9] or learnable parameter [8]. In ConvPoint, the correlation functions H_m are defined as the m -th component of the output of an MLP, namely $H_m(x - y) = \text{MLP}_m \left([(x - y) - c_m]_{m=1}^M \right)$, where square brackets denote concatenation. In KPConv, each H_m is an RBF, namely a function $H_m(x - y) = h(\|(x - y) - c_m\|)$ that differs from the others only by the parameter $c_m \in \mathbb{R}^d$.

In Fig. 2(b) we illustrate the operations of the point-convolutional layers ConvPoint [8] and KPConv [9] in terms of matrix multiplications. The linear combination in (2) can be expressed as a multiplication between the weight tensor $\tilde{W} = (\tilde{w}_{ijm})$ and the matrix H stacking the values of correlation functions $H_m(x - y)$ for $x \in X_y$ and $m \in \{1, \dots, M\}$. Then, each output feature $\psi_j(y)$ can be expressed as the Frobenius inner product between the matrix Φ containing the input features $\phi_i(x)$ for $x \in X_y$ and $i \in \{1, \dots, I\}$, and the j -th slice of $\tilde{W}H$.

V. PROPOSED APPROACH

We propose the *composite layer*, a new point-convolutional operator. Our composite layer is defined by composing a *spatial function* $s : \mathbb{R}^d \rightarrow \mathbb{R}^K$, which extracts the spatial information from the coordinates of the points in X_y , and a *semantic function* $f(\phi, s)$ that combines the output of s with all the input features $\{\phi(x) : x \in X_y\}$ to produce the output feature vector $\psi(y)$, see Fig. 1. From a very general perspective, our composite layer can be written as:

$$\psi_j(y) = f_j(\phi, s)(y). \quad (3)$$

In what follows we show that this formulation provides additional regularization and has superior design flexibility compared to the existing point-convolutional layers.

A. Convolutional Composite Layer

As in ConvPoint, in our *convolutional composite layer* we randomly sample each output point $y \in Q$ from the input point cloud P , and define the convolution windows X_y by nearest neighbors. This choice guarantees that all the windows contain the same number of points, making point convolution more efficient and easier to implement.

Spatial Function. Inspired by [9], [11], we implement the spatial function s using a Radial Basis Function Network (RBFN) with M centers, which in principle has the same approximation capability of MLPs [51] but depends on fewer hyperparameters. Similarly to the filters g_{ij} in point-convolutional layers (1), the K components of the spatial function take as input the relative position of each point $x \in X_y$ with respect

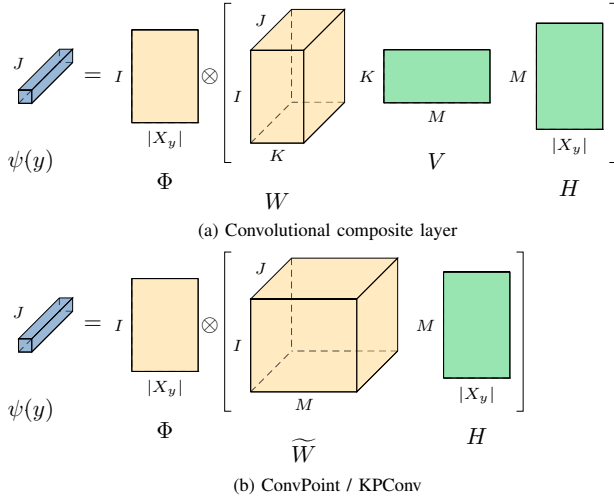


Fig. 2. The scheme illustrating the operations in point-convolutional layers expressed in matrix form. (a) Our convolutional composite layer (5); (b) the well-known point-convolutional layers ConvPoint and KPConv. Here \otimes indicates the Frobenius inner product. In practice, our composite layer decomposes the matrix \widetilde{W} of ConvPoint and KPConv into the product $W \cdot V$, enabling more flexibility in terms of number of parameters.

to the location of the output point y . We define the k -th component of s as:

$$s_k(x - y) = \sum_{m=1}^M v_{km} h(\|(x - y) - c_m\|), \quad (4)$$

where v_{km} are learnable parameters, for $k \in \{1, \dots, K\}$. We employ a Gaussian function $h(r) = \exp(r^2/2\sigma^2)$, where $r = \|(x - y) - c_m\|$, σ is a hyperparameter common to all RBFs as in [11]. The position of the centers $\{c_m\}$ is learned during training. The spatial function can be expressed as a multiplication between a weight matrix $V = (v_{km})$ and the matrix H , which contain the RBF output $h(\|(x - y) - c_m\|)$ for each point $x \in X_y$ and RBF center c_m for $m \in \{1, \dots, M\}$, as shown in Fig. 2(a). Thus, the spatial function compresses the spatial information by projecting each column of H to a K -dimensional space, where $K < M$ is a hyperparameter.

Semantic Function. To produce an equivalent formulation of point convolution (1) from our composite layer (3) we define the semantic function as:

$$\psi_j(y) = f_j(\phi, s)(y) = \sum_{x \in X_y} \sum_{i=1}^I \phi_i(x) \underbrace{\sum_{k=1}^K w_{ijk} s_k(x - y)}_{g_{ij}(x-y)}, \quad (5)$$

where the indices i, j, k refer to the i -th component of the input feature vector, the j -th output feature vector and the k -th component of the spatial function, and w_{ijk} are learnable parameters. As shown in Fig. 2(a), the most inner sum in (5) can be expressed as a multiplication of the projections VH against each of the J slices of a tensor $W = (w_{ijk})$, which contains the learnable weights of each convolution filter. Finally, each output feature $\psi_j(y)$ can be expressed as the Frobenius inner product between the matrix Φ containing the features $\phi_i(x)$ for $x \in X_y$ and $i \in \{1, \dots, I\}$ and the j -th slice of WVH .

Comparison with point-convolutions. The formulation of our composite convolution is equivalent to point convolution since the most inner sum in (5) can be interpreted as the filter function g_{ij} in (1). In Fig. 2 we compare the matrix operations of our convolutional composite layer with two mainstream point-convolutional layers, namely ConvPoint [8] and KPConv [9]. When applied to a convolution window X_y , all these layers combine the input features of the points $x \in X_y$, grouped in the matrix Φ , and the spatial information extracted from the coordinates of the points encoded in the matrix H . While our layer extracts the spatial information in H by the spatial function (4) and then shares it among the filters (5), KPConv and ConvPoint directly learn a huge weight tensor \widetilde{W} to combine spatial information and features.

Therefore, our convolutional composite layer has two major advantages over the existing point-convolutional layers: *i*) it performs an implicit regularization by decomposing \widetilde{W} into the product $W \cdot V$, which has lower rank than \widetilde{W} , and *ii*) it is more flexible since it allows to increase the complexity (and therefore the descriptive power) of the spatial function without dramatically increasing the number of parameters of the layer, as we show in Section V-D. In particular, the complexity of the spatial function can be tuned by increasing the number of RBF centers M . Similarly, in KPConv and ConvPoint, the number of centers M allows to tune the complexity of the network processing the coordinates of the points $x \in X_y$. However, the size of \widetilde{W} , which collects the vast majority of the parameters of KPConv and ConvPoint layers, grows linearly with M , while in our composite layer only the size of V , which contains substantially fewer parameters than \widetilde{W} , grows with M (see Fig. 2).

B. Aggregate Composite Layer

We also define an *aggregate composite layer*, implementing a nonlinear semantic function f that aggregates the spatial information extracted by s (4) and the input features ϕ differently from point-convolution (1). In particular, we adopt pooling operators defined as the component-wise mean \mathcal{M}_s and standard deviation \mathcal{S}_s of the output of the spatial function over the points $x \in X_y$, namely:

$$\begin{aligned} [\mathcal{M}_s(y)]_k &= \frac{1}{|X_y|} \sum_{x \in X_y} s_k(x - y), \\ [\mathcal{S}_s(y)]_k &= \sqrt{\frac{\sum_{x \in X_y} (s_k(x - y) - [\mathcal{M}_s(y)]_k)^2}{|X_y| - 1}}. \end{aligned}$$

Thus, the pooling functions \mathcal{M}_s and \mathcal{S}_s receive as input $|X_y|$ vectors in \mathbb{R}^K (the output of the spatial function s), and return a single vector in \mathbb{R}^K each. Analogously, we define $\mathcal{M}_\phi(y), \mathcal{S}_\phi(y) \in \mathbb{R}^I$ as the component-wise mean and standard deviation of the features of the points in the convolution window X_y . Then, we concatenate these in two vectors $\theta(y) = [\mathcal{M}_s(y); \mathcal{S}_s(y)] \in \mathbb{R}^{2K}$ and $\eta(y) = [\mathcal{M}_\phi(y); \mathcal{S}_\phi(y)] \in \mathbb{R}^{2I}$, and combine them as:

$$f_j(\phi, s)(y) = \theta(y)^\top W_j \eta(y) = \sum_{i=1}^{2I} \sum_{k=1}^{2K} \theta_k(y) w_{ijk} \eta_i(y), \quad (6)$$

TABLE I
THE ARCHITECTURE EMPLOYED IN ALL OUR EXPERIMENTS FOR BOTH
OUR CONVOLUTIONAL AND AGGREGATE COMPOSITE NETS.

Layer Type	J	$ X_y $	$ Q $
Composite + BN + ReLU	J_0	32	1024
Composite + BN + ReLU	$2 \cdot J_0$	32	256
Composite + BN + ReLU	$4 \cdot J_0$	16	64
Composite + BN + ReLU	$4 \cdot J_0$	16	16
Composite + BN + ReLU	$8 \cdot J_0$	16	1
Dense	-	-	-

where W_j is a slice of the weight tensor $W = (w_{ijk})$. Since the two vectors $\theta(y), \eta(y)$ are obtained by concatenating the mean and standard deviation over the window X_y , this semantic function is nonlinear. In terms of the matrix multiplication in Fig. 2(a), our aggregate composite layer combines the columns of VH to extract a unique spatial descriptor for X_y and does the same for Φ , before computing the Frobenius product. Our aggregate layer forces the network to learn from the mean and standard deviation (6) of the points coordinates in X_y and of the features in Φ , thus introducing an additional form of regularization.

C. CompositeNet

We implement a simple neural network \mathcal{N} , called CompositeNet, consisting of 5 composite layers. A scheme illustrating our architecture is shown in Table I, which reports the number of output features J , the window cardinality $|X_y|$ and the number of output points $|Q|$ for each layer. We chose these parameters so that our architecture is equivalent to the deep neural network based on ConvPoint layers proposed in [8]. The number of output features J of each layer is defined relatively to the number of output features J_0 of the first layer, which is a hyperparameter. Nonlinearities and batch normalization are applied only to the features and not to the spatial coordinates of the points: this is similar to what happens in CNNs for images, where the spatial coordinates of pixels are not modified. The cardinality of the point cloud is reduced throughout the network by sampling, in each layer, fewer output points than input points. From the last composite layer, we obtain a single point with a feature vector and feed this to a dense layer, discarding its coordinates.

Using the architecture illustrated in Table I, we implement a convolutional CompositeNet based on our convolutional composite layer (Section V-A) and an aggregate one based on our aggregate composite layer (Section V-B). We train our CompositeNets for point cloud classification and, most remarkably, anomaly detection following the self-supervised approach proposed in [17], which we briefly illustrate here. Starting from a training set containing only point clouds from a given normal class, we form a new self-annotated dataset by applying N different geometric transformations $\{\mathcal{T}_0, \dots, \mathcal{T}_{N-1}\}$ to the point clouds of the training set, where \mathcal{T}_0 is the identity. Then, we train a CompositeNet \mathcal{N} to classify

the transformations applied to each input point cloud. The rationale behind [17] is that, while learning to distinguish geometric transformations, the network learns features that are useful for anomaly detection. During testing, we apply the same transformations to each point cloud P and classify the resulting point clouds $\mathcal{T}_n(P)$ by \mathcal{N} . Then, we use as normality score the average posterior probability (according to \mathcal{N}) of the correct transformations applied to P , i.e.

$$S(P) = \frac{1}{N} \sum_{n=0}^{N-1} [\mathcal{N}(\mathcal{T}_n(P))]_n. \quad (7)$$

This method was first designed for 2D images, so the geometric transformations included rotations, translations and flips [17], which cannot be straightforwardly adopted on 3D point clouds since virtually all neural networks for point clouds are insensitive to translations. Moreover, most real-world objects (e.g. chairs, tables, etc.) have a common vertical orientation and thus appear arbitrarily rotated around the vertical axis in the training set. For this reason, we employ a set of $N = 8$ rotations of an angle $\alpha \in \{0^\circ, 45^\circ, 90^\circ, 135^\circ, 210^\circ, 240^\circ, 300^\circ, 330^\circ\}$ around a fixed horizontal axis, including the identity (a rotation of 0°).

D. Design Flexibility

In Sections V-A and V-B we show that our composite layer encompasses both point-convolutional layers and operators that aggregate spatial information and features in a nonlinear manner. Here we investigate the superior design flexibility granted by our composite layers in terms of number of parameters compared to ConvPoint [8] and KPConv[9]. In particular, we perform two experiments to show that, contrarily to ConvPoint and KPConv, we can easily customize the spatial and semantic components and thus *i)* improve the classification performance without increasing the overall number of parameters, and *ii)* reduce the number of parameters by of our CompositeNets without compromising their performance.

Tuning the complexity of the spatial function. In the first experiment, we train different configurations of our CompositeNets on the ScanNet dataset [5], tuning the number of centers $M \in \{8, 16, \dots, 256\}$ to modify the number of parameters of the spatial function. We compare our CompositeNets with the original ConvPoint network, which has the same architecture as ours. We also implement a KPConv network having the same architecture as our CompositeNets. We call this *KPConv-vanilla* to distinguish it from the model in [9], which has a way more sophisticated architecture including residual blocks. In ConvPoint and KPConv-vanilla, we tune $M \in \{8, 16, \dots, 256\}$ as in our CompositeNets.

As remarked in Section V-A, in ConvPoint and KPConv layers the number of parameters increases linearly with M , which determines the size of the weight tensor \bar{W} . In contrast, when tuning M in our composite layers, we only modify the complexity of the spatial function, i.e. the size of the weight matrix V . The output dimension K of the spatial function is instead fixed (we set $K = 16$) thus the size of the weight tensor W , which contains most of the learnable parameters, does not increase with M .

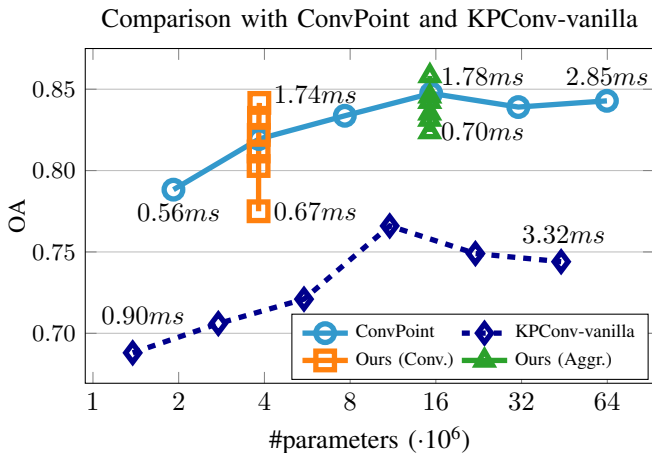


Fig. 3. Overall accuracy on ScanNet varying the complexity of the spatial function by tuning $M \in \{8, 16, \dots, 256\}$, against the number of parameters of the network. We also report the average time to process a point cloud during training with the least and most complex configurations. The parameters of ConvPoint and KPConv-vanilla double with M (note that the scale is logarithmic), while in our CompositeNets M can be increased without significantly changing the number of parameters (there is an increase of $< 1\%$ passing from $M = 8$ to $M = 256$).

Fig. 3 shows the overall accuracy (OA) over the ScanNet dataset against the number of parameters of the networks. In ConvPoint and KPConv-vanilla the number of parameters doubles with M , while in our CompositeNets it increases less than 1% when passing from $M = 8$ to $M = 256$. In our CompositeNets, the accuracy increases with M , while ConvPoint and KPConv-vanilla achieve their best performance at $M = 64$ and yield worse accuracy at $M = 128, 256$, suggesting that they might be more prone to overfitting due to the increased number of parameters. KPConv-vanilla performs substantially worse than our CompositeNets and ConvPoint, suggesting that KPConv layers cannot be successfully employed in simple architectures and that the excellent performance of KPConv [9] is probably due to its sophisticated architecture.

For the least and most complex network configurations based on each layer, we report the average processing time of a point cloud during training. We observe that, in all cases, the processing time increases with M due to the increasing complexity of the spatial component. However, in ConvPoint and KPConv-vanilla the processing time increases more than in our CompositeNets due to the linear growth of the number of parameters with respect to M .

We obtain similar results on the synthetic ModelNet40 [18] and ShapeNetCore [19] datasets, where our CompositeNets achieve similar results when setting $M = 64, 128, 256$. Therefore, on these datasets we set $M = 64$ to reduce the processing time while obtaining approximately the same classification performance. The results in Fig. 3 demonstrate that increasing the complexity of our spatial function by setting a larger M can substantially improve the performance of our CompositeNets on challenging, real-world datasets such as ScanNet [5] without requiring a larger number of parameters. **Tuning the number of parameters.** In the second experiment, we train different configurations of our CompositeNets on the ModelNet40 dataset [18]. In this case, we investigate how

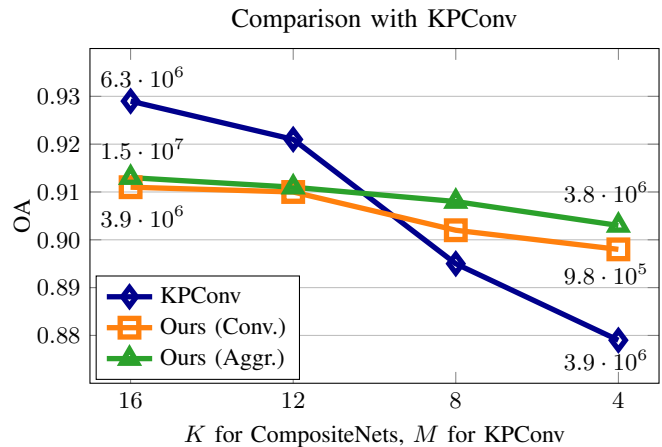


Fig. 4. Overall accuracy on ModelNet40 when reducing the number of parameters by tuning K (M for KPConv). We also report the number of parameters of the most and least complex configurations. These results show that we can substantially reduce the parameters of our CompositeNets without compromising the accuracy, while this is not the case in KPConv.

the classification accuracy varies after reducing the number of parameters by tuning the output dimension of the spatial function $K \in \{16, 12, 8, 4\}$. We compare the accuracy of our CompositeNets with that achieved by the original KPConv [9] varying the number of centers $M \in \{16, 12, 8, 4\}$. In KPConv, M plays a similar role as K in our composite layers since it regulates the size of the weight tensor \bar{W} , which contains the majority of the layer parameters (see Fig. 2(b)).

Fig. 4 shows the overall accuracy of each network and the overall number of parameters of the most and least complex configurations of each network. Although KPConv achieves the best performance overall (when $M = 16$), its accuracy gets substantially worse when reducing the number of parameters by setting $M = 8$ and $M = 4$. On the other hand, both our convolutional and aggregate composite layers retain better performance for low K . These results highlight the flexibility of our composite layers, which allows to substantially reduce the number of parameters (-75% passing from $K = 16$ to $K = 4$) without compromising the accuracy, which decreases by approximately 0.01. In fact, the smaller number K of spatial function components is counterbalanced by a constant number of centers, which we set to $M = 16$ in all the experiments. In contrast, the accuracy of KPConv is extremely sensitive to M (-0.05 passing from $M = 16$ to $M = 4$), which is the only hyperparameter we can tune to reduce the number of parameters of a KPConv layer. Moreover, the reduction in the number of parameters is less substantial compared to our CompositeNets (-38% passing from $M = 16$ to $M = 4$) due to the more sophisticated architecture. In fact, tuning M does not change the number of parameters of the residual blocks.

VI. EXPERIMENTS

Our experiments are meant to show the effectiveness of composite layers in deep neural networks for point clouds. In particular, we address classification and, most remarkably, unsupervised anomaly detection by training our CompositeNets in a self-supervised fashion [17].

TABLE II
HYPERPARAMETERS OF OUR CONVOLUTIONAL AND AGGREGATE
COMPOSITENETS, CONVPOINT AND KPConv-VANILLA MAXIMIZING THE
VALIDATION ACCURACY ON EACH CONSIDERED DATASET.

Dataset	Layer	J_0	M	K
ModelNet40 [18]	Ours (Conv.)	64	64	16
	Ours (Aggr.)	64	64	16
	ConvPoint	64	16	–
	KPConv-vanilla	64	16	–
ShapeNetCore [19]	Ours (Conv.)	32	64	16
	Ours (Aggr.)	32	64	16
	ConvPoint	32	16	–
	KPConv-vanilla	64	32	–
ScanNet [5]	Ours (Conv.)	64	256	32
	Ours (Aggr.)	64	256	32
	ConvPoint	64	32	–
	KPConv-vanilla	64	64	–

A. Benchmarking Datasets

We adopt two well-known synthetic 3D classification benchmarks: *ModelNet40* [18], which contains 12,311 objects from 40 classes, and a subset of *ShapeNet* [19] called *ShapeNet-Core*, which contains 51,127 shapes from 55 rather imbalanced classes. Both datasets contain 3D meshes, from which we sample point clouds of 1024 points, setting a constant feature function $\phi \equiv 1$. This is a standard procedure to build point clouds containing only spatial information [6], [9].

We also perform our experiments on real-world data using shapes extracted from the *ScanNet-v2* dataset [5], which contains 1513 3D scenes (obtained from RGB-D scans) of 707 indoor environments with instance-level annotations of 608 classes. Specifically, we extract the meshes of objects belonging to the 17 most populated classes (excluding planar objects such as windows, walls and doors) as in the classification experiments in [5], and sample 1024 points from each object, as for the synthetic datasets. The resulting dataset is severely imbalanced. Moreover, the objects are often partially occluded since they were acquired from real-world scenes.

In the classification experiments, we train each network with all the classes contained in the official training split of each dataset. The same splits are used in our anomaly detection experiments, where the networks are trained in an unsupervised fashion, i.e. only over instances from a single class that is considered normal. During testing, point clouds from any other class are considered anomalous. Since training deep neural networks require relatively large training sets to extract meaningful features, in our anomaly detection experiments we consider exclusively point clouds from the 7 most represented classes from *ShapeNet* (at least 2000 instances, as in [16]) and the 14 largest classes from *ScanNet* (at least 400 instances).

B. Multiclass Classification

We train our CompositeNets for 200 epochs on an NVIDIA RTX A6000 GPU. We use the Adam optimizer [52] and the traditional cross-entropy loss for multiclass classification. In Table II we report the hyperparameter configurations of

our CompositeNets we selected to maximize the validation accuracy on each dataset.

Considered methods. We compare our CompositeNets against PointNet [6], KPConv [9], and ConvPoint [8], reporting their accuracy on ModelNet40 from the corresponding papers. Since the performance on ShapeNetCore and ScanNet were not reported, we train and test the competing networks using the software implementations made publicly available. We remark that both our CompositeNets are equivalent to ConvPoint in terms of architecture, and have a comparable number of parameters. This makes the comparison between the performance of our CompositeNets and ConvPoint particularly significant. In contrast, PointNet uses a custom non-convolutional architecture and KPConv uses a deeper residual network, making both models significantly different from ours. We also train KPConv-vanilla, namely a network based on KPConv layers having the same architecture as our CompositeNets. In Table II we report the configuration of ConvPoint proposed in [8] for ModelNet40, and the configurations we selected for ConvPoint and KPConv-vanilla to maximize the validation accuracy also on the other datasets. KPConv layers have an additional hyperparameter with respect to ConvPoint, namely the radius ρ defining the convolution windows [9]. In KPConv-vanilla we have tuned ρ in a $\pm 20\%$ range compared to the value in [9] without obtaining substantial changes in the accuracy.

Figures of merit. As performance metrics we consider overall accuracy (OA), defined as the proportion of correctly classified point clouds, and average accuracy (AA), namely the average per-class accuracy, which better takes into account the accuracy on under-represented classes. We train each method 5 times and compute the average OA and AA, except for the results on ModelNet40, which we report from [6], [8], [9].

Experimental results. The results in Table III indicate that our CompositeNets achieve comparable performance to ConvPoint [8] and KPConv [9] on all the considered datasets. Therefore, the point-convolutional layers in these models can be successfully replaced by our composite layers, which are more flexible, as shown in Section V-D. Moreover, the poor performance of KPConv-vanilla confirms that, contrarily to ours, KPConv layers require a sophisticated residual architecture to achieve good classification accuracy.

Here we illustrate these results more in detail. On ModelNet40 [18], our CompositeNets approach ConvPoint [8] both in terms of overall and average accuracy, and substantially outperform PointNet [6] in terms of overall accuracy. KPConv yields the best overall accuracy, but we could not report its average accuracy since this result is not reported in [9]. On ShapeNetCore [19], our aggregate CompositeNet yields the best OA, slightly outperforming ConvPoint, while our convolutional CompositeNet performs similarly to PointNet and KPConv. Our aggregate CompositeNet yields also the best AA, which is particularly important on imbalanced datasets such as ShapeNetCore since it better evaluates the accuracy over classes with fewer samples. On ScanNet [5] our aggregate CompositeNet performs very similarly to KPConv, which has a slightly better OA. Also in this case, our aggregate CompositeNet yields the best AA, suggesting that our aggregate CompositeNet is more robust to class imbalance than other

TABLE III

OVERALL (OA) AND AVERAGE ACCURACY (AA). THE RESULTS OF COMPETING METHODS ON MODELNET40 ARE FROM THE LITERATURE (KPCONV [9] DOES NOT REPORT THE AA), WHILE THE RESULTS ON SHAPENETCORE AND SCANNET ARE OBTAINED USING THE AVAILABLE CODE.

Dataset	PointNet [6]		KPCConv [9]		KPCConv-vanilla		ConvPoint [8]		Ours (Conv.)		Ours (Aggr.)	
	OA	AA	OA	AA	OA	AA	OA	AA	OA	AA	OA	AA
ModelNet40 [18]	0.892	0.862	0.929	–	0.879	0.848	0.918	0.885	0.913	0.871	0.911	0.879
ShapeNetCore [19]	0.830	0.686	0.829	0.671	0.752	0.632	0.837	0.669	0.828	0.653	0.839	0.698
ScanNet [5]	0.786	0.751	0.878	0.835	0.766	0.699	0.847	0.811	0.861	0.824	0.871	0.839

methods. Remarkably, our aggregate CompositeNet outperforms ConvPoint on challenging datasets such as ShapeNet-Core and ScanNet and achieves similar accuracy to KPCConv despite having a much simpler architecture. We also observe that, while PointNet achieves good results on the synthetic ModelNet40 and ShapeNetCore datasets, its performance on the real-world ScanNet dataset is substantially worse than the other models. On all the considered datasets, our convolutional CompositeNet performs similarly to ConvPoint, but worse than our aggregate CompositeNet and than KPCConv.

C. Unsupervised Anomaly Detection

We train our self-supervised CompositeNets for 200 epochs on an NVIDIA RTX A6000 GPU. We use the Adam optimizer [52], and the same network configurations selected for our classification experiments on each dataset (Table II).

Considered methods. Since we are among the first to address anomaly detection in point clouds, we consider a shallow baseline that relies on hand-crafted features, somewhat similarly to [3], [15]. In particular, we use the *Global Orthographic Object Descriptor* (GOOD) [53] to compress the salient characteristics of each point cloud into a feature vector. Compared to most of the existing point cloud descriptors [20], the advantage of GOOD is that it can be directly employed on point clouds that contain only the coordinates of the points, and do not require additional features such as the orthonormal vectors to the surface at each point. To perform anomaly detection, we first use GOOD to extract a feature vector from each normal point cloud in the training set. Then, we use these feature vectors to train an *Isolation Forest* (IFOR) [54], a well-known outlier-detection algorithm that we employ at test time to identify anomalous point clouds.

To the best of our knowledge, the only work using deep learning for anomaly detection in point clouds is [16], in particular, a variational autoencoder (VAE) based on FoldingNet [49]. Since the implementation of this method is not publicly available, we report the results on the 7 most numerous classes of the ShapeNet dataset that were published in [16]. We also compare our self-supervised CompositeNets with KPCConv [9] and ConvPoint [8], trained in the same fashion using the same architectures as in classification. We recall that our CompositeNets have a simple architecture like ConvPoint, while KPCConv has a deeper, residual architecture. We do not consider KPCConv-vanilla in this experiment because of its poor performance in multiclass classification.

Figures of merit. We assess the anomaly detection performance by the Area Under the ROC Curve (AUC), which

measures how well each network can distinguish normal instances from the anomalous ones. Following [55], we report the average rank of each method over the classes and the p-values of the one-sided Wilcoxon Signed-Rank test assessing whether the performance difference between the best-ranking method and the others is statistically significant.

Experimental results. In Table IV we report the results of our experiments. On ShapeNet, self-supervised deep neural networks outperform both the shallow baseline IFOR and the VAE [16] in most of the classes and in terms of average rank. However, the Wilcoxon test [55] comparing our aggregate CompositeNet (which is the best-performing method in terms of average rank) and these baselines yields p-value > 0.05 , probably due to the fact that the number of considered classes is small. Unfortunately, we could not compare our CompositeNets with the VAE [16] on more classes from ShapeNet since its implementation is not publicly available.

On ScanNet, all methods tend to perform worse than they do on the synthetic data from ShapeNet. We expected this result since the real-world objects in ScanNet are often partially occluded. Also in this case, we observe that self-supervised deep neural networks outperform IFOR in most of the classes. Our aggregate CompositeNet is the best-performing method in most classes and in terms of average rank, and the Wilcoxon test [55] confirms that the difference with all the other methods, except for KPCConv, is statistically significant (p-value ≤ 0.05). These results show that our aggregate CompositeNet substantially outperforms ConvPoint in both the considered datasets, and performs similarly to KPCConv despite having a much simpler architecture.

Finally, we observe that applying IFOR to feature vectors extracted by GOOD yields relatively good performance on a small number of classes, outperforming deep solutions on the *Lamp* and *Sofa* classes from ShapeNet, and on the *Book* and *Towel* classes from ScanNet. However, IFOR yields poor performance on most of the other classes, often achieving $AUC \leq 0.5$. This suggests that point cloud descriptors cannot characterize well all classes of point clouds, thus deep learning can address anomaly detection in a more general way.

D. Discussion and Limitations

Our classification and anomaly detection experiments show that our aggregate CompositeNet outperforms ConvPoint and achieves similar results as KPCConv despite having a much simpler architecture. The performance of our convolutional CompositeNet is slightly worse, on par with ConvPoint. We believe that these promising results can be further improved

TABLE IV

ANOMALY DETECTION PERFORMANCE (AUC) OF OUR SELF-SUPERVISED COMPOSITENETS, TWO SIMILAR NETWORKS BASED ON CONVPOINT [8] AND KPConv [9], AND A SHALLOW DETECTOR BASED ON THE GOOD DESCRIPTOR [53]. WE ALSO REPORT THE RESULTS OBTAINED BY THE VARIATIONAL AUTOENCODER IN [16] ON SHAPENET. BOLD DENOTES THE BEST AUC FOR EACH CLASS. OUR AGGREGATE COMPOSITENET IS THE BEST-PERFORMING METHOD ON MOST CLASSES AND IN TERMS OF AVERAGE RANK.

Class		Baseline IFOR	SOTA VAE [16]	Self-supervised deep neural networks			
				KPConv	ConvPoint	Ours (Conv.)	Ours (Aggr.)
ShapeNet [19]	Airplane	0.912	0.747	0.974	0.956	0.969	0.970
	Car	0.712	0.757	0.988	0.953	0.953	0.972
	Chair	0.571	0.931	0.921	0.910	0.904	0.941
	Lamp	0.962	0.907	0.372	0.373	0.391	0.424
	Table	0.883	0.839	0.943	0.777	0.821	0.854
	Rifle	0.475	0.382	0.967	0.976	0.978	0.977
	Sofa	0.986	0.777	0.923	0.898	0.936	0.944
Avg. Rank		3.714	4.429	2.857	4.357	3.500	2.143
Wilcoxon-p		$2.89 \cdot 10^{-1}$	$1.09 \cdot 10^{-1}$	$3.44 \cdot 10^{-1}$	$7.81 \cdot 10^{-3}$	$2.34 \cdot 10^{-2}$	–
ScanNet [5]	Backpack	0.677	–	0.851	0.778	0.783	0.779
	Book	0.830	–	0.734	0.731	0.782	0.782
	Bookshelf	0.745	–	0.796	0.792	0.824	0.798
	Box	0.429	–	0.705	0.638	0.630	0.659
	Cabinet	0.581	–	0.813	0.818	0.810	0.827
	Chair	0.449	–	0.747	0.842	0.837	0.838
	Desk	0.482	–	0.869	0.857	0.870	0.888
	Lamp	0.540	–	0.639	0.707	0.703	0.725
	Pillow	0.647	–	0.693	0.707	0.754	0.771
	Sink	0.415	–	0.896	0.892	0.921	0.940
	Sofa	0.785	–	0.876	0.859	0.852	0.852
	Table	0.318	–	0.920	0.912	0.902	0.902
	Towel	0.801	–	0.657	0.690	0.640	0.655
	Trash Can	0.426	–	0.881	0.918	0.921	0.927
Avg. Rank		4.727	–	2.000	3.227	3.273	1.773
Wilcoxon-p		$1.46 \cdot 10^{-3}$	–	$6.50 \cdot 10^{-1}$	$2.53 \cdot 10^{-3}$	$9.28 \cdot 10^{-3}$	–

by implementing more sophisticated architectures based on our composite layers.

We speculate that the good performance of our CompositeNets is due to the superior design flexibility of our models, which enables the design of rich spatial functions that boost the layer’s capability to recognize local spatial relations between points. Moreover, the performance difference between our aggregate and convolutional CompositeNets suggests that a non-convolutional aggregation might be beneficial. In contrast, existing point-convolutional layers such as ConvPoint and KPConv cannot be customized without substantially changing the overall number of parameters of the network (see Fig. 3) or taking the risk of decreasing their performance (see Fig. 4). The flexibility in customizing the number of parameters can be crucial when training sets are small (as in our anomaly detection experiments), which increases the risk of overfitting.

We are among the first to address unsupervised deep anomaly detection on point clouds. The self-supervised approach [17] we employed to train our CompositeNets for anomaly detection only enables discriminating between normal and anomalous point clouds, and cannot be directly used to detect anomalous regions within a point cloud. This is an emerging problem whose first benchmark has been recently released [56], and that we will address in future works.

Although very effective, the self-supervised anomaly detection approach [17] has another fundamental limitation since, as noted in [43], the transformations applied to the training set are domain-dependent, and most transformations used for images are not suited for point clouds. Moreover, the selected

set of transformations might not be well suited for some of the possible normal classes, resulting in poor anomaly detection performance. For instance, all the considered self-supervised neural networks achieve $AUC < 0.5$ on the class *Lamp* from the ShapeNet dataset. We speculate that this result is due to the fact that said class contains both table and ceiling lamps, which makes it hard to distinguish the rotations applied lamps having different vertical orientations. In contrast, the VAE [16] and GOOD [53] can apparently extract relevant features from these point clouds, and therefore yield better anomaly-detection performance on the class *Lamp* from ShapeNet [19]. All in all, our experiments confirm that the self-supervised approach proposed in [17] is extremely effective as long as the geometric transformations are carefully chosen depending on the considered normal class. When that is not the case, as for the class *Lamp* from ShapeNet [19], other algorithms might perform better. In general, the great flexibility of our composite layers and the promising results obtained by our models in the anomaly-detection task encourage us to continue our research and employ our CompositeNets also for other unsupervised tasks.

VII. CONCLUSIONS AND FUTURE WORK

We introduce the composite layer, an effective solution to design deep neural networks for point clouds enabling more flexibility in terms of design and number of parameters than existing point-convolutional layers such as KPConv and ConvPoint. Our experiments show that CompositeNets achieve classification and anomaly-detection performance on par with

KPConv despite having a simpler architecture and outperform ConvPoint, which instead has the same architecture as our CompositeNets. Moreover, our results show that self-supervised networks perform substantially better than shallow baselines leveraging hand-crafted point cloud descriptors and existing anomaly-detection algorithms for point clouds based on variational autoencoders.

Future work will address the implementation of more sophisticated CompositeNets, leveraging deeper, residual architectures that comprise both convolutional and aggregate composite layers, with the aim of improving classification and anomaly-detection performance. To address the intrinsic limitations of the self-supervised approach in [17], we will investigate how to automatically learn suitable transformations directly from the point clouds of the training set as in [45], where such transformations have been successfully learned for signals and images. We will also design CompositeNets able to detect anomalous regions within point clouds, to be tested on upcoming real-world datasets such as [56]. Another research direction that combines the design flexibility of our composite layer and the self-supervised approach is unsupervised hyperparameter tuning and pre-training for 3D deep learning [57], [58], which are of paramount importance since annotated 3D datasets are not as large and widespread as 2D image datasets.

ACKNOWLEDGMENT

The authors gratefully acknowledge the support of NVIDIA with the four RTX A6000 GPUs granted to Politecnico di Milano through the Applied Research Accelerator Program.

REFERENCES

- [1] B. Yang, W. Luo, and R. Urtasun, "Pixor: Real-time 3d object detection from point clouds," in *IEEE Conference on Computer Vision and Pattern Recognition*, 2018, pp. 7652–7660.
- [2] Y. Cui, R. Chen, W. Chu, L. Chen, D. Tian, Y. Li, and D. Cao, "Deep learning for image and point cloud fusion in autonomous driving: A review," *IEEE Transactions on Intelligent Transportation Systems*, 2021.
- [3] Z. Ao, Y. Su, W. Li, Q. Guo, and J. Zhang, "One-class classification of airborne LiDAR data in urban areas using a presence and background learning algorithm," *Remote Sensing*, vol. 9, no. 10, p. 1001, 2017.
- [4] S. Teruggi, E. Grilli, M. Russo, F. Fassi, and F. Remondino, "A hierarchical machine learning approach for multi-level and multi-resolution 3d point cloud classification," *Remote Sensing*, vol. 12, no. 16, p. 2598, 2020.
- [5] A. Dai, A. X. Chang, M. Savva, M. Halber, T. Funkhouser, and M. Nießner, "ScanNet: Richly-annotated 3d reconstructions of indoor scenes," in *IEEE Conference on Computer Vision and Pattern Recognition*, 2017, pp. 5828–5839.
- [6] C. R. Qi, H. Su, M. Kaichun, and L. J. Guibas, "Pointnet: Deep learning on point sets for 3d classification and segmentation," in *IEEE Conference on Computer Vision and Pattern Recognition*, 2017, pp. 77–85.
- [7] Y. Guo, H. Wang, Q. Hu, H. Liu, L. Liu, and M. Bennamoun, "Deep learning for 3d point clouds: A survey," *IEEE Transactions on Pattern Analysis and Machine Intelligence*, vol. 43, no. 12, pp. 4338–4364, 2021.
- [8] A. Boulch, "ConvPoint: Continuous convolutions for point cloud processing," *Computers & Graphics*, vol. 88, pp. 24–34, 2020.
- [9] H. Thomas, C. R. Qi, J.-E. Deschaud, B. Marcotegui, F. Goulette, and L. J. Guibas, "KPConv: Flexible and deformable convolution for point clouds," in *IEEE International Conference on Computer Vision*, 2019, pp. 6411–6420.
- [10] C. R. Qi, L. Yi, H. Su, and L. J. Guibas, "Pointnet++: Deep hierarchical feature learning on point sets in a metric space," in *31st International Conference on Neural Information Processing Systems*, 2017.
- [11] M. Atzmon, H. Maron, and Y. Lipman, "Point convolutional neural networks by extension operators," *ACM Transactions on Graphics*, vol. 37, no. 4, 07 2018.
- [12] Y. Xu, T. Fan, M. Xu, L. Zeng, and Y. Qiao, "SpiderCNN: Deep learning on point sets with parameterized convolutional filters," in *European Conference on Computer Vision*. Springer, 2018, pp. 87–102.
- [13] W. Chen, X. Han, G. Li, C. Chen, J. Xing, Y. Zhao, and H. Li, "Deep RBFNet: Point cloud feature learning using radial basis functions," *arXiv preprint arXiv:1812.04302*, 2018.
- [14] J. Lyu and S. Manoochehri, "Online convolutional neural network-based anomaly detection and quality control for fused filament fabrication process," *Virtual and Physical Prototyping*, vol. 16, no. 2, pp. 160–177, 2021.
- [15] B. Rodríguez-Cuenca, S. García-Cortés, C. Ordóñez, and M. C. Alonso, "Automatic detection and classification of pole-like objects in urban point cloud data using an anomaly detection algorithm," *Remote Sensing*, vol. 7, no. 10, pp. 12 680–12 703, 2015.
- [16] M. Masuda, R. Hachiuma, R. Fujii, H. Saito, and Y. Sekikawa, "Toward unsupervised 3d point cloud anomaly detection using variational autoencoder," in *2021 IEEE International Conference on Image Processing (ICIP)*. IEEE, 2021, pp. 3118–3122.
- [17] I. Golan and R. El-Yaniv, "Deep anomaly detection using geometric transformations," in *32nd International Conference on Neural Information Processing Systems*, 2018, pp. 9781–9791.
- [18] Z. Wu, S. Song, A. Khosla, F. Yu, L. Zhang, X. Tang, and J. Xiao, "3d shapenets: A deep representation for volumetric shapes," in *IEEE Conference on Computer Vision and Pattern Recognition*, 2015, pp. 1912–1920.
- [19] A. X. Chang, T. Funkhouser, L. Guibas, P. Hanrahan, Q. Huang, Z. Li, S. Savarese, M. Savva, S. Song, H. Su, J. Xiao, L. Yi, and F. Yu, "ShapeNet: An Information-Rich 3D Model Repository," *Technical Report arXiv:1512.03012 [cs.GR]*, 2015.
- [20] X.-F. Hana, J. S. Jin, J. Xie, M.-J. Wang, and W. Jiang, "A comprehensive review of 3d point cloud descriptors," *arXiv preprint arXiv:1802.02297*, vol. 2, 2018.
- [21] C. R. Qi, H. Su, M. Nießner, A. Dai, M. Yan, and L. Guibas, "Volumetric and multi-view CNNs for object classification on 3D data," in *IEEE Conference on Computer Vision and Pattern Recognition*, 2016.
- [22] L. Ge, H. Liang, J. Yuan, and D. Thalmann, "Robust 3d hand pose estimation from single depth images using multi-view CNNs," *IEEE Transactions on Image Processing*, vol. 27, no. 9, pp. 4422–4436, 2018.
- [23] C. Choy, J. Gwak, and S. Savarese, "4d spatio-temporal convnets: Minkowski convolutional neural networks," in *IEEE/CVF Conference on Computer Vision and Pattern Recognition*, 2019, pp. 3075–3084.
- [24] B. Graham, M. Engelcke, and L. Van Der Maaten, "3d semantic segmentation with submanifold sparse convolutional networks," in *IEEE Conference on Computer Vision and Pattern Recognition*, 2018, pp. 9224–9232.
- [25] S. Wang, S. Suo, W.-C. Ma, A. Pokrovsky, and R. Urtasun, "Deep parametric continuous convolutional neural networks," in *IEEE Conference on Computer Vision and Pattern Recognition*, 2018, pp. 2589–2597.
- [26] W. Wu, Z. Qi, and L. Fuxin, "PointConv: Deep convolutional networks on 3d point clouds," in *IEEE/CVF Conference on Computer Vision and Pattern Recognition*, 2019, pp. 9621–9630.
- [27] F. Yang, H. Wang, and Z. Jin, "Adaptive GMM convolution for point cloud learning," in *British Machine Vision Conference*, 2021.
- [28] J. Mao, X. Wang, and H. Li, "Interpolated convolutional networks for 3d point cloud understanding," in *IEEE/CVF International Conference on Computer Vision*, 2019, pp. 1578–1587.
- [29] Y. Lin, Z. Yan, H. Huang, D. Du, L. Liu, S. Cui, and X. Han, "Fpconv: Learning local flattening for point convolution," in *IEEE/CVF Conference on Computer Vision and Pattern Recognition*, 2020, pp. 4293–4302.
- [30] Y. Liu, B. Fan, S. Xiang, and C. Pan, "Relation-shape convolutional neural network for point cloud analysis," in *IEEE/CVF Conference on Computer Vision and Pattern Recognition*, 2019, pp. 8895–8904.
- [31] H. Ran, W. Zhuo, J. Liu, and L. Lu, "Learning inner-group relations on point clouds," in *IEEE/CVF International Conference on Computer Vision*, 2021, pp. 15477–15487.
- [32] Y. Liu, B. Fan, G. Meng, J. Lu, S. Xiang, and C. Pan, "DensePoint: Learning densely contextual representation for efficient point cloud processing," in *IEEE/CVF International Conference on Computer Vision*, 2019, pp. 5239–5248.
- [33] M. Xu, R. Ding, H. Zhao, and X. Qi, "PAConv: Position adaptive convolution with dynamic kernel assembling on point clouds," in *IEEE/CVF Conference on Computer Vision and Pattern Recognition*, 2021, pp. 3173–3182.
- [34] F. Gama, A. G. Marques, G. Leus, and A. Ribeiro, "Convolutional neural network architectures for signals supported on graphs," *IEEE Transactions on Signal Processing*, vol. 67, no. 4, pp. 1034–1049, 2018.

- [35] Y. Wang, Y. Sun, Z. Liu, S. E. Sarma, M. M. Bronstein, and J. M. Solomon, "Dynamic graph CNN for learning on point clouds," *ACM Transactions On Graphics*, vol. 38, no. 5, pp. 1–12, 2019.
- [36] W. Hu, X. Gao, G. Cheung, and Z. Guo, "Feature graph learning for 3d point cloud denoising," *IEEE Transactions on Signal Processing*, vol. 68, pp. 2841–2856, 2020.
- [37] M. Feng, S. Z. Gilani, Y. Wang, L. Zhang, and A. Mian, "Relation graph network for 3d object detection in point clouds," *IEEE Transactions on Image Processing*, vol. 30, pp. 92–107, 2020.
- [38] B. Paaßen, D. Grattarola, D. Zambon, C. Alippi, and B. E. Hammer, "Graph edit networks," in *International Conference on Learning Representations*, 2021.
- [39] X. Ma, C. Qin, H. You, H. Ran, and Y. Fu, "Rethinking network design and local geometry in point cloud: A simple residual MLP framework," in *International Conference on Learning Representations*, 2022.
- [40] C. Zhou and R. C. Paffenroth, "Anomaly detection with robust deep autoencoders," in *ACM SIGKDD International Conference on Knowledge Discovery and Data Mining*, 2017, pp. 665–674.
- [41] D. T. Nguyen, Z. Lou, M. Klar, and T. Brox, "Anomaly detection with multiple-hypotheses predictions," in *International Conference on Machine Learning*. PMLR, 2019, pp. 4800–4809.
- [42] L. Ruff, R. Vandermeulen, N. Goernitz, L. Deecke, S. A. Siddiqui, A. Binder, E. Müller, and M. Kloft, "Deep one-class classification," in *International Conference on Machine Learning*, vol. 80. PMLR, 2018, pp. 4393–4402.
- [43] S. Goyal, A. Raghunathan, M. Jain, H. V. Simhadri, and P. Jain, "DROCC: Deep robust one-class classification," in *International Conference on Machine Learning*. PMLR, 2020, pp. 3711–3721.
- [44] D. M. Tax and R. P. Duin, "Support vector data description," *Machine Learning*, vol. 54, no. 1, pp. 45–66, 2004.
- [45] C. Qiu, T. Pfrommer, M. Kloft, S. Mandt, and M. Rudolph, "Neural transformation learning for deep anomaly detection beyond images," in *International Conference on Machine Learning*. PMLR, 2021, pp. 8703–8714.
- [46] L. Ruff, J. R. Kauffmann, R. A. Vandermeulen, G. Montavon, W. Samek, M. Kloft, T. G. Dietterich, and K.-R. Müller, "A unifying review of deep and shallow anomaly detection," *Proceedings of the IEEE*, vol. 109, no. 5, pp. 756–795, 2021.
- [47] M. Zamorski, M. Zieba, P. Klukowski, R. Nowak, K. Kurach, W. Stokowiec, and T. Trzciński, "Adversarial autoencoders for compact representations of 3d point clouds," *Computer Vision and Image Understanding*, vol. 193, p. 102921, 2020.
- [48] Y. Zhao, T. Birdal, H. Deng, and F. Tombari, "3d point capsule networks," in *IEEE/CVF Conference on Computer Vision and Pattern Recognition*, 2019, pp. 1009–1018.
- [49] S. Chen, C. Duan, Y. Yang, D. Li, C. Feng, and D. Tian, "Deep unsupervised learning of 3d point clouds via graph topology inference and filtering," *IEEE Transactions on Image Processing*, vol. 29, pp. 3183–3198, 2019.
- [50] P. Hermosilla, T. Ritschel, P.-P. Vázquez, À. Vinacua, and T. Ropinski, "Monte Carlo convolution for learning on non-uniformly sampled point clouds," *ACM Transactions on Graphics*, vol. 37, no. 6, pp. 1–12, 2018.
- [51] J. Park and I. W. Sandberg, "Universal approximation using radial-basis-function networks," *Neural Computation*, vol. 3, no. 2, pp. 246–257, 1991.
- [52] D. P. Kingma and J. Ba, "Adam: A method for stochastic optimization," in *International Conference on Learning Representations*, 2015.
- [53] S. H. Kasaei, A. M. Tomé, L. S. Lopes, and M. Oliveira, "GOOD: A global orthographic object descriptor for 3D object recognition and manipulation," *Pattern Recognition Letters*, vol. 83, pp. 312–320, 2016.
- [54] F. T. Liu, K. M. Ting, and Z.-H. Zhou, "Isolation forest," in *IEEE International Conference on Data Mining*. IEEE, 2008, pp. 413–422.
- [55] J. Demšar, "Statistical comparisons of classifiers over multiple data sets," *Journal of Machine Learning Research*, vol. 7, no. Jan, pp. 1–30, 2006.
- [56] P. Bergmann, X. Jin, D. Sattlegger, and C. Steger, "The MVTEC 3D-AD dataset for unsupervised 3D anomaly detection and localization," in *17th International Joint Conference on Computer Vision, Imaging and Computer Graphics Theory and Applications (VISAPP)*. SciTePress, 2022, pp. 202–213.
- [57] S. Xie, J. Gu, D. Guo, C. R. Qi, L. Guibas, and O. Litany, "PointContrast: Unsupervised pre-training for 3d point cloud understanding," in *European Conference on Computer Vision*. Springer, 2020, pp. 574–591.
- [58] Z. Zhang, R. Girdhar, A. Joulin, and I. Misra, "Self-supervised pre-training of 3d features on any point-cloud," in *IEEE/CVF International Conference on Computer Vision*, 2021, pp. 10 252–10 263.



Alberto Floris graduated in Computer Science and Engineering at Politecnico di Milano in 2021. He is currently a Data Scientist at Skykraft AB (Sweden), where he develops machine learning algorithms for large-scale LiDAR point clouds.



Luca Frittoli graduated in Mathematics at Università degli Studi di Milano in 2018, and is currently working towards the Ph.D. in Information Technology at Politecnico di Milano. His research interests include change detection in multivariate datastreams, concept-drift detection, and deep learning methods for anomaly detection and open-set recognition in images and point clouds.



in signal and images, and domain adaptation.

Diego Carrera graduated in Mathematics at Università degli Studi di Milano in 2013 and received the Ph.D. in Information Technology in 2018. In 2015 he has been visiting researcher at the Tampere University of Technology. Currently he is an Application Development Engineer at STMicroelectronics, where he is developing quality inspection systems to monitor the wafer production. His research interests are mainly focused on unsupervised learning algorithms, in particular change detection in high dimensional datastreams, anomaly detection



Giacomo Boracchi is an Associate Professor of Computer Engineering at Politecnico di Milano - DEIB, where he also received the Ph.D. in Information Technology (2008), after graduating in Mathematics (Università degli Studi di Milano, 2004). His research interests concern machine learning and image processing, and in particular change/anomaly detection, domain adaptation, image restoration and analysis. Since 2015 he is leading industrial research projects concerning outlier detection systems, X-ray systems, and automatic quality inspection systems.

He has published more than 70 papers in international conferences and journals, he is currently associate editor for IEEE Transactions on Image Processing and in 2019 - 2020 he served as an associate editor for IEEE Computational Intelligence Magazine. In 2015 he received an IBM Faculty Award, in 2016 the IEEE Transactions on Neural Networks and Learning Systems Outstanding Paper Award, in 2017 the Nokia Visiting Professor Scholarship, and in 2021 the NVIDIA Applied Research Grant. He has held tutorials in major IEEE conferences: ICIP 2020, ICASSP 2018, and IJCNN 2017 and 2019.